Thin Solid Films 734 (2021) 138865

Contents lists available at ScienceDirect

Thin Solid Films

journal homepage: www.elsevier.com/locate/tsf

Hydrophobic Silica Thin Film derived from Dimethyldimethoxysilane-Tetraethylorthosilicate for Desalination

Adi Darmawan *, Linda Karlina, Ika Khairunnisak, Riza Eka Saputra, Choiril Azmiyawati, Yayuk Astuti, S. Sriatun, Avior Puspa Noorita

Department of Chemistry, Diponegoro University, Semarang 50275, Indonesia

ARTICLE INFO

Keywords:
Hydrophobicity
Silica
Dimethyldimethoxysilane
Desalination
Membrane

ABSTRACT

Silica thin film preparation was carried out from dimethyldimethoxysilane (DMDMS) and tetraethylorthosilicate (TEOS) precursors using the sol-gel method, and the effect of pH on the character of the resulting silica membrane was also studied. The solution pH was varied into 2.21; 3.92; 4.98; 6.44; and 7.21. The resulting xerogel was analyzed using Fourier-transform infrared spectroscopy, Thermogravimetric Analysis, and Gas Sorption Analysis. While the silica thin layer was measured for its hydrophobic character and surface morphology using Scanning Electron Microscope. The presence of DMDMS-TEOS silica thin film had a considerable influence on the hydrophobic nature of the ceramic plate surface. The membrane prepared under neutral conditions produced desirable properties, such as higher thermal stability, greater pore volume, thermal stability, and higher hydrophobicity. For the desalination process, the obtained silica membrane showed excellent separation performance (>99%), especially at low salt concentrations. When the pH increased, the water flux also increased. The thin films worked well for desalination through a pervaporation mechanism.

1. Introduction

Many regions worldwide are suffering from freshwater scarcity, experiencing limited access to fresh water and proper sanitation. Currently, there is a great need to obtain clean water from sophisticated natural-based sources. Recent developments have made it possible to produce fresh water from the sea or brackish water through a membrane filtering process. Membrane technology is highly remarkable as its efficiency can save energy far better than conventional distillation techniques [1]. Moreover, membrane technology has high operational stability, requires lower-cost materials, ease of network integration, and ease of control for industrial processes [1]. For desalination purposes, there are currently three types of membrane technology used, i.e. (i) reverse osmosis (RO) membrane, (ii) membrane distillation, and (iii) pervaporation [2]. RO is currently the most widely used desalination membrane technology, mainly because it was first discovered, and the installation and operation costs are more economical for this technology [3]. In recent years, pressure-free membrane processes, such as pervaporation, have acceded much attention [4]. In several studies, pervaporation has shown to produce a good performance. Salt rejection by pervaporation is excellent, reaching above 99%, especially for monovalent salt [5, 6].

Furthermore, as pervaporation is different from reverse osmosis, which uses pressure, phase changes can occur without surmounting the salt feed osmotic pressure. This implies that pervaporation can be carried out to desalinate water with high salt concentration without increasing the driving force. Silica membranes specifically attract attention because their fabrication techniques are simple, have relatively low costs, and generate excellent molecular sieving properties, as demonstrated in gas molecule separation [7, 8].

The microporous silica membrane has a molecular sieve structure in which the pore size is within the kinetic diameter of the species to be separated (dp = 3–5 Å). In desalination with membrane pervaporation, the membrane pore width must be larger in diameter than water molecules (d_k = 2.6 Å) but smaller than hydrated salt ions (e.g., Na^+: d_k = 7.2 Å and Cl^-: d_k = 6.6 Å) [9]. Silica membrane synthesis primarily uses the sol-gel method in which the reaction occurs in a solvent and involves hydrolysis and condensation reactions [10]. The silanol (Si-OH) group on the silica membrane formed from the hydrolysis is hydrophilic and makes the silica membrane unstable when exposed to water. When exposed to water, the silica matrix can experience damage and/or densification [11], which leads to the enlargement of pore size. As such,

* Corresponding author.
E-mail address: adidarmawan@live.undip.ac.id (A. Darmawan).

https://doi.org/10.1016/j.tsf.2021.138865
Received 10 December 2020; Received in revised form 27 July 2021; Accepted 27 July 2021
Available online 30 July 2021

the separation performance will decrease and ultimately degrade the desalinated water quality. Modification of silica membrane is, thus, imperative to improve hydrothermal stability [12]. Strategies for silica surface functionalization have been reported, including the incorporation of structural stabilizing groups, such as hydrophobic groups [13], carbonized polymer [14, 15], surfactant templates [16, 17], organosilica [18], and metal oxides [19–21]. The incorporation of a hydrophobic group -CH_3 on silica by co-condensation of tetraethylorthosilicate (TEOS) and methyltriethoxysilane H_3C-Si$(OEt)_3$ has formerly been studied [13, 22]. The material showed good hydrostability and was helpful for the pervaporation of organic compounds [23]. Wei et al. [24] described using (trifluoropropyl)triethoxysilane to create a hydrophobic silica membrane. However, the use of this hydrophobic precursor was mostly for gas membrane applications. Dimethyldimethoxysilane (DMDMS) was recently used to make hydrophobic thin films because it has methyl and methoxy groups [25, 26] and provided good surface hydrophobicity properties. Similarly, the pH effect on hydrolysis kinetics and the resulting silica properties have been investigated [27]. The sol pH is one of the main parameters that influence the final structural formation of the desired silica thin layer. It controls the speed of hydrolysis and condensation reactions [28].

The present paper reports the manufacture of a hydrophobic distillation membrane from DMDMS-TEOS via a sol-gel method for water desalination purposes. The pH variation was performed to find out the effect of pH on hydrophobicity and desalination performance. The membrane supports were modified with DMDMS to be hydrophobic and suitable for desalination. Sol-gel solutions were characterized using the zeta potential. Silica thin films were characterized using contact angle characterization, Fourier transforms infrared spectroscopy (FTIR), Thermogravimetric Analysis (TGA), Gas Sorption Analysis (GSA), and Scanning Electron Microscope (SEM) to illustrate the silica membrane characteristics. The synthesized silica thin film membrane was tested under desalination at different salt concentrations and feed temperatures. This work's key finding is the formulation of the relationship between the pH of hydrophobic silica synthesis and desalination performance. This work also presents that increase in water flux and selectivity were manifested in membranes synthesized at low pH.

2. Experimental section

The silica sol was prepared by hydrolysis and condensation of tetraethylorthosilicate (TEOS, Merck, 99% pure) with dimethyldimethoxysilane (DMDMS, Aldrich, 98% pure) catalyzed with various pH in ethanol (Merck, 99% pure) solvent. The ethanol solvent was conditioned with acetic acid (Merck, 99% pure) at 1 M, 0.25 M, 0.025 M, without acetic acid, and with 0.1 M ammonia solution (Merck). DMDMS followed by TEOS was carefully added to the ethanol solution under stirring using a magnetic stirrer for 45 min in an ice bath to avoid fractional hydrolysis whereby the final pH of each was pH 2.21, 3.92, 4.98, 6.44, and 7.21, respectively, as shown in Table 1. The final reaction mixture had a molar ratio of DMDMS: TEOS: ethanol = 0.1: 0.1: 10. The resulting mixture solution was then divided into two parts, one part was used for silica thin layer preparation, and the other part was dried into xerogel for characterization.

Xerogel was made by evaporating the solution at room temperature for a week, and then the sample was dried in an oven at 60 °C under normal atmospheric conditions. Xerogel samples were mashed and sieved with a 100-mesh (150 μm) sieve, followed by calcination at 350 °C for 2 h at a ramp rate of 2 °C min^{-1} under standard atmosphere. The silica membrane was applied by coating silica sols onto the macroporous α-alumina (Al_2O_3) substrates (ϕ≈10 mm, purity 96%, Ceramic Oxide Fabricates Australia) through a dip coating process of the substrate into the silica sol with a soaking time of 2 min and the immersion and withdrawal rate of 10 cm min^{-1}. Then, each coated alumina substrate was calcined separately at 350 °C and 500 °C in a temperature-controlled furnace, with a dwell time of 2 h and a ramp rate of 2 °C min^{-1}. The drying conditions, temperature and heating rate were the same for both the thin layers and the xerogels. The dip-coating and calcination procedure was repeated four times to obtain a thicker hydrophobic film on the membrane support and avoid cracking in the thin film. Silica sols were also coated on a commercial ceramic plate to measure thin films' hydrophobicity by measuring the water contact angle. The same treatment, coating, and calcination conditions were applied to the ceramic plates and membrane supports.

Zeta potential values of silica sol-gel solution were evaluated using Malvern Zetasizer Nano ZSP to determine the electric potential in the interfacial double layer (DL) relative to a point in the bulk fluid away from the interface of the silica sol-gel. The functional groups of hydrophobic silica xerogels were identified using the Shimadzu IRAffinity-1 Fourier-transform infrared (FTIR) spectrometer with the Pike MIRacle the wavelength range of 400–4000 cm^{-1}. To obtain quantitative information, all spectra were normalized to the highest peak at 1080 cm^{-1}. To analyze the silica framework, spectra in the 900–1300 cm^{-1} region were deconvoluted using the Fityk program on each sample with the Gaussian approach [26, 29]. The same number of peaks was used in the deconvoluted spectra. Half-width at half maximum (HWHM) was fixed at each peak, while the peak position was allowed to change slightly to obtain a model curve that was as close as possible to the original spectra.

Xerogel thermal analysis was carried out using a Shimadzu TGA-50 thermogravimetric analyzer with atmospheric air, an airflow rate of 60 mL min^{-1}, and a heating rate of 2 °C min^{-1} from room temperature to 800 °C. For nitrogen adsorption analysis, xerogels (~0.2 g) were degassed under vacuum (10^{-6} mbar) for more than 6 h at 125 °C before analysis with the TriStar 3020 Micromeritic instrument at 77 K (−196 °C). Pure N_2 (99.9%) gas was used. Porous properties were determined by analyzing the N_2 adsorption/desorption data using MicroActive Software for TriStar II. The specific surface area was determined using the brunauer, emmett, and teller (BET) method in the relative pressure range $0.05 < P/P^{\circ} < 0.25$, where the total pore volume was taken from the last point of the isotherm. The average pore diameter was calculated with 4 V/A from the BET value. Pore size distribution (PSD) was estimated by the MP-Method. The thin layer morphology was visualized using the scanning electron microscope (SEM) Phenom Pro-X desktop SEM operated at 10 kV acceleration voltage in which samples prepared under acidic and alkaline conditions were placed on clean aluminum stubs.

The measurement of water contact angle (WCA) was carried out using the tan $\theta/2$ method. Deionized water was carefully dropped using a syringe on the thin layer surface coated on a ceramic plate. Geometrically, WCA was calculated as $\theta/2 = \tan^{-1}(h/r)$, where r is the water droplet's radius, and h is the water droplet peak height. The WCA value was determined by measuring and calculating the average WCA from three water drops dripped onto different positions on the same plate.

Desalination tests on silica thin-film membranes were carried out by measuring the water flux and the percentage of rejected salt concentrations. The membrane assembly referred to the classic pervaporation design for desalination as described elsewhere [21]. The silica thin film membrane was immersed in a beaker containing a sodium chloride solution (NaCl, Sigma Aldrich) with concentrations varying from 0.3, 1, and 3.5 wt.% at feedwater temperatures of 15 °C, 30 °C, and 45 °C. One end of the membrane tube was blocked, and the other end was connected to a cold trap (immersed in a water-ice bath) and a vacuum pump

Table 1
pH of solution in the DMDMS-TEOS silica synthesis.

The concentration of acids or bases in ethanol solvent	the final pH of the solution
1 M acetic acid	2.21
0.25 M acetic acid	3.92
0.025 M acetic acid	4.98
Ethanol without the addition of acid or base	6.44
0.1 M ammonia	7.21

at 1.5 kPa.

The water flux, F (kg $m^{-2} j^{-1}$), was determined based on the equation $F = m/(A.\Delta t)$, where m is the permeate mass (kg) condensed in the cold trap, A is the active surface area (m^2) of the silica thin film membrane, and Δt is the measurement time (h). Salt rejection, R (%), was calculated as $R = R = \frac{(C_f - C_p)}{C_f} \times 100\%$, where C_f is the concentration of salt in the feed, and C_p is the concentration of salt in the permeate. The salt concentration was determined from conductivity measurements referring to the standard curves made using the total dissolved solids meter.

3. Results and discussion

3.1. Zeta potential

In Fig. 1, DMDMS-TEOS silica sol-gel prepared at the most acidic pH shows the highest zeta potential. The zeta potential gradually decreases with increasing pH. The zeta potential value is determined by the equilibrium between the OH^- group and the silanol group of the silica framework. Because the silica framework has Si-OH groups which at high OH^- concentrations ionize to Si-O^-, the increase in the OH^- content in the solution decreases the zeta potential. Although the zeta potential value fluctuates, there is a strong correlation between the zeta potential value and pH, which is indicated by the R^2 correlation coefficient value, which is more than 9.

3.2. Hydrophobicity of DMDMS-TEOS silica thin films

The average water contact angles (WCA) of DMDMS-TEOS silica thin films coated on ceramic plates were obtained, as shown in Fig. 2. The WCA study was performed for silica thin films calcined at 350 °C and 500 °C under various pH conditions of DMDMS-TEOS solution, i.e., 2.21, 3.92, 4.98, 6.44, and 7.21. The WCA analysis was used to investigate the hydrophobicity of membrane surfaces coated by DMDMS-TEOS silica thin films. The contact angle depends directly on the interaction of the droplet contact line with the surface, wherein the more chemically hydrophobic the material is, the higher the resulting angle.

The ceramic plate that was not coated by a silica thin layer had a water contact angle of 36° This indicates that the ceramic plate surface was initially hydrophilic. The contact angle increased dramatically when the ceramic plates were coated with silica. The water contact angle produced is attributed to the silica's low surface energy generated by the -Si(CH_3) group on the silica thin layer [30]. Fig. 2 shows that there are differences in water droplet size at each pH and calcination temperature. The higher the DMDMS-TEOS sol-gel pH, the greater the contact angle for all calcination temperatures. The WCA from pH = 2.21 to 6.44 showed a trend of notable increase. However, the WCA value increased significantly at pH of 6.44 to 7.21. This indicates that the silica thin layer gradually became hydrophobic by increasing the pH, which is

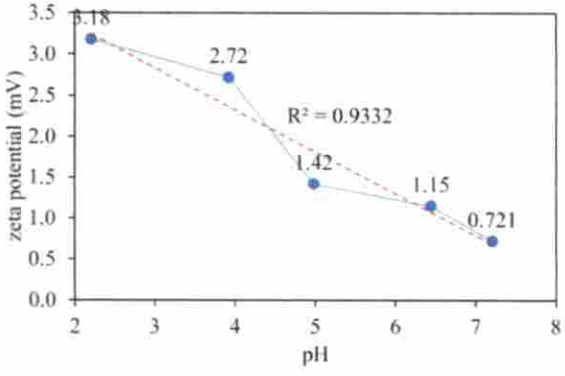

Fig. 1. The zeta potential DMDMS-TEOS silica sol gel as a function of pH.

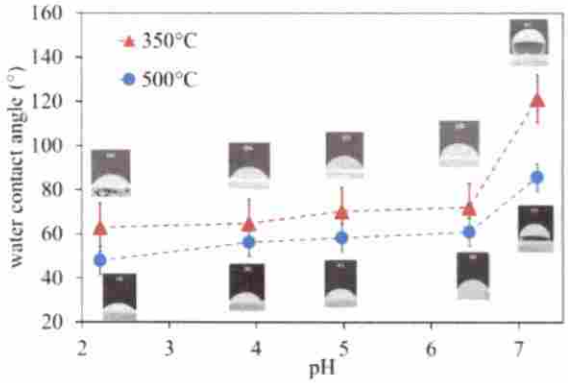

Fig. 2. The water contact angle of DMDMS-TEOS silica thin films coated on ceramic plates calcined at 350 °C and 500 °C as a function of pH.

in line with previous reports [31]. Hysteresis from a high contact angle shows that the surface hydrophobicity followed Wenzel's state [32]. For all samples, the varied results for contact angle were caused by the glass surface's silanization that had given rise to surface roughness and hydrophobic chemical functional groups. Indeed, the results show that pH can manipulate contact angle because it creates a different chemical environment.

The phenomena observed might have manifested because, at a higher pH, the silica condensation process proceeded faster than the hydrolysis process; therefore, the polymer chains formed would be more branched and caused the formed thin film to become rougher. A higher pH also resulted in a chemical environment that encouraged DMDMS to replace hydroxyl groups, especially at pH 7. This was demonstrated by the sharp increase in contact angle at pH 7. Meanwhile, at low pH, long-chain silica would be formed and give rise to a smoother surface. Roughness in surface morphology leads to the rise of surface hydrophobicity [33].

Fig. 2 shows that silica calcined at 350 °C always had higher contact angles than that calcined at 500 °C for all pH variations. The silica thin layer contains many hydroxyl and siloxane groups, each responsible for the hydrophilic and hydrophobic character of the film surface [26]. At 500 °C calcination temperature, the hydroxyl group underwent a condensation reaction to form a siloxane group, and the methyl group's oxidation process took place. The formation of siloxanes and the loss of methyl groups reduced the silica surface's hydrophobic nature [25]. These results are further explained by FTIR and TGA data presented later.

3.3. Fourier transform infrared analysis

FTIR analysis was performed on DMDMS-TEOS silica xerogel to determine the silica functional groups and other types of functional groups by bond type analysis. It is assumed that the xerogel and thin layer have the same character. The analysis was carried out with the xerogel as it was difficult to observe the characteristics of the thin layers. Fig. 3(a) shows the FTIR spectra recorded in the range 1300–750 cm^{-1}. A band peak at 1260 cm^{-1} is directly correlated to the symmetrical vibrations of the CH group [34], whereas stretching Si-O-Si in the silica structure can be seen in the range of 1000–1200 cm^{-1} (asymmetrical vibrations) and at 800 cm^{-1} (symmetrical vibrations) [25, 29]. Furthermore, a peak of 860 cm^{-1} indicates the symmetrical vibration from the Si-C group, and the 960 cm^{-1} peak denotes the symmetrical vibration from Si-OH [35].

Based on the FTIR spectra of DMDMS-TEOS shown in Fig. 3(a), similar shape and intensity of absorption peaks at the wavenumbers of 1000–1200 cm^{-1} were observed in all pH. Overall, the spectral form for silica xerogels calcined at 350 °C and 500 °C looks similar regardless of pH variations. This reveals that no significant change in the silica's

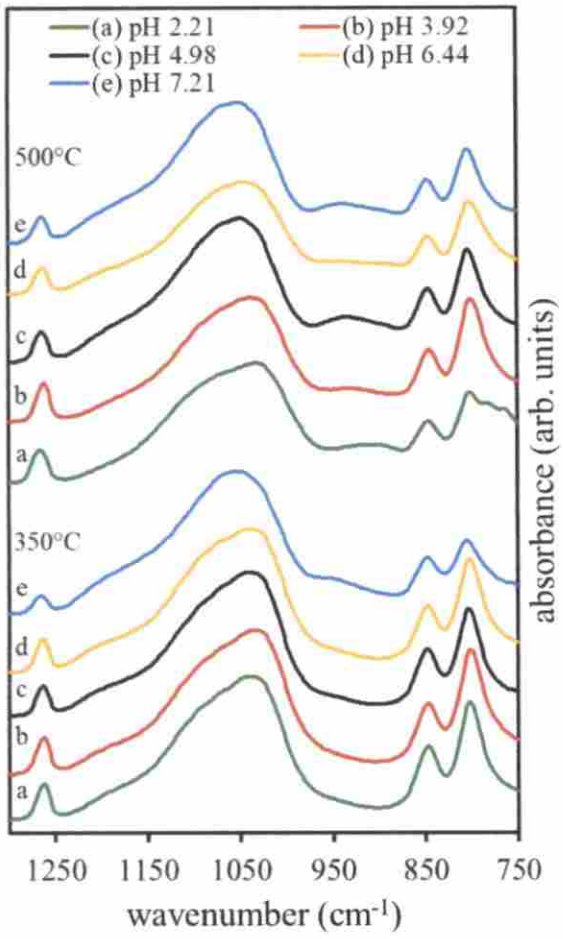

Fig. 3. FTIR spectra of DMDMS-TEOS silica xerogels calcined at 350 °C and 500 °C as a function of pH.

functional groups occurred due to variation in pH. However, a significant difference of reduced absorbance at the peak of 860 cm^{-1} associated with Si-C vibrations was observed. The decrease in absorbance marked the decrease in the number of methyl groups due to calcination at a higher temperature.

To provide more in-depth information, deconvolution to the FTIR spectra was performed. The deconvolution was achieved using the Gaussian peak components on the FTIR spectra performed on the wavenumbers between 800 and 1300 cm^{-1}, as shown in Fig. 4(a). The deconvolution of FTIR spectra was carried out to distinguish the number of bands present. From the FTIR spectra, there were eight bands obtained. Correlatively, deconvolution calculations were described elsewhere [26] on Si-OH, Si-CH_3, CH, and Si-O-Si groups. It was found that there was a correlation between the (cyclic Si-O-Si)/(linear Si-O-Si) ratio and the hydrophobic properties of the silica thin film surface. Subsequently, the deconvolution in this study was also focused on the 1030 cm^{-1} and 1080 cm^{-1} regions, connoting the asymmetrical vibration of linear Si-O-Si and cyclic Si-O-Si groups, respectively [26, 36].

The cyclic Si-O-Si ring is generally stable to hydrolysis and is the most significant part of silica oligomers obtained from TEOS derivatives. Thus, it was expected that the cyclic siloxane becomes dominant in the silica polymers. Confirmedly, this was indicated by the relatively high peak intensity at 1080 cm^{-1}. The cyclic Si-O-Si groups tend to be more hydrophobic than linear Si-O-Si, meaning that the cyclic Si-O-Si component is more in amount than the linear Si-O-Si component, then the silica thin layer will be more hydrophobic [26, 37]. The area of the two peak components was thus calculated as the ratio (cyclic

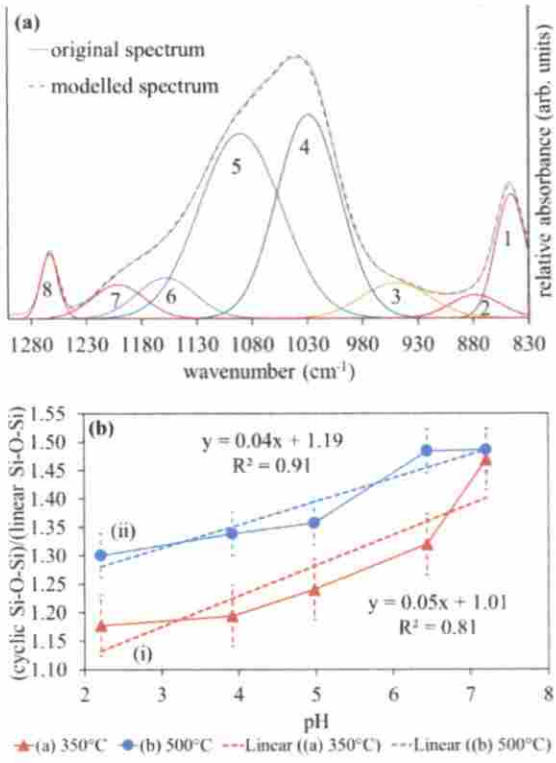

Fig. 4. (a) Deconvoluted FTIR spectra, spectra 1 to 8 are derived spectra obtained from the deconvolution of the original spectra, (b) DMDMS-TEOS (cyclic Si-O-Si/linear Si-O-Si) ratio of silica xerogel calcined at (i) 350 °C and (ii) 500 °C as a function of pH. The dotted lines indicate a linear trendline.

Si-O-Si)/(Si-O-Si linear) shown in Fig. 4(b). The ratio (cyclic Si-O-Si)/(linear Si-O-Si) tends to increase with increasing pH. The linear trendline is marked with a dotted line showing the correlation between the ratio (cyclic Si-O-Si)/(linear Si-O-Si) and pH. The R^2 (coefficient of determination) values are 0.81 and 0.91 for the silica thin films calcined at 350 °C and 500 °C, respectively. Although not high, the value of the coefficient of determination indicates a cooperative relationship between pH and the ratio (cyclic Si-O-Si)/(linear Si-O-Si). These results indicate that the cyclical and linear siloxane compositions significantly affect the hydrophobic properties of silica. If more cyclic silica groups are present, the more hydrophobic the silica surface is. Besides the siloxane bridge, another group contributing to hydrophobicity is the Si (CH_3) group. However, deconvolution calculations did not show any quantitative correlation between the area of the Si(CH_3) group and pH.

3.4. Thermogravimetric analysis

The thermogravimetric analysis (TGA) and derivative thermogravimetry (DTG) results depict the gradual mass loss of xerogels, as shown in Fig. 5. TGA results showed a mass loss of about 10–13% for heating up to 800 °C. The decline in mass percentage was observed to have occurred in three degradation steps. The first was related to residual solvent and volatile components in the samples lost in the temperature up to 200 °C. The second was dehydroxylation caused by the OH group condensation reaction, which resulted in the Si-O-Si group (200 to 350 °C) [21, 38, 39]. The third was the decomposition of methyl groups and the remaining neighboring hydroxyl groups (350° to 600 °C) [37]. The TGA result is presented starting at the temperature of 100 °C to minimize the appearance of residual solvent and volatile components in the samples.

TGA and DTG curves show that variations in pH produced different thermal stability. Based on the curve shapes, the TGA curves can be

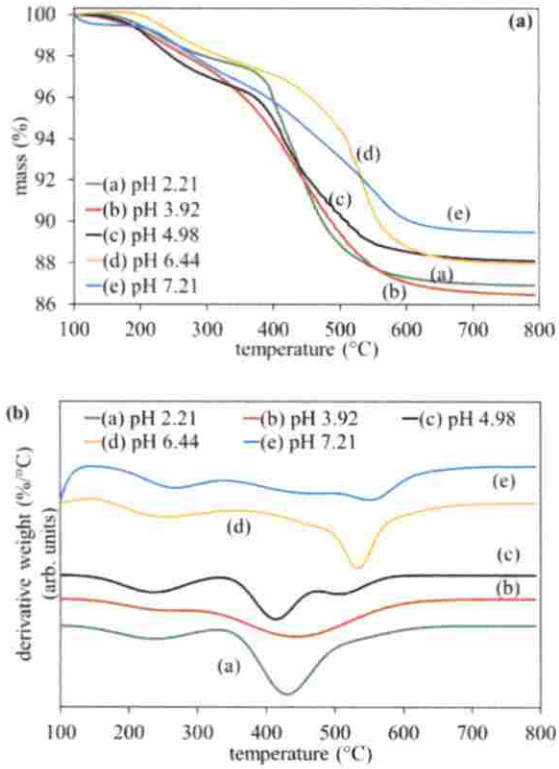

Fig. 5. (a) TGA and (b) DTG of DMDMS-TEOS silica xerogels at various pH conditions.

grouped into two, i.e., the first being samples prepared at pH 2.21, 3.92, and 4.98, where they show a similar TGA curve shape and the second being samples prepared from pH 6.44 and 7.21, both of which show similar patterns that differ from the more acidic samples. Samples prepared at pH up to 5 yield the same silica structure, and thus their degradation patterns tended to be similar. The results are in line with the hydrophobicity data in which up to pH = 5, only a slight change occurred. The DTG data shows that the maximum decomposition temperature (peak temperature at which the fastest weight loss rate occurred) was in the range of 400 °C-500 °C. The DTG peak in this region revealed the existence of organic matter. Organic constituents decompose at around 400 °C and at a maximum of 450 °C.

However, for samples with a pH of 6.44 and above, pH appeared to have played a significant role in the constituting structure of the materials produced. Hydrolysis and condensation reactions are affected by acid and alkaline conditions. Under acidic conditions, condensation occurs between silanol groups located on the monomers or ends of the polymer. Conversely, under alkaline conditions, the condensation reaction occurs in the most acidic (most likely deprotonated) silanol bonds of the Q^3 Si atom [40]. Moreover, the alcoholysis reaction is much faster under alkaline conditions than under acidic conditions. This causes the $Si(CH_3)$ group to be better protected under alkaline conditions. This reinforced the nitrogen adsorption results in which the sample prepared at pH 7.21 experienced a doubling of the amount of nitrogen absorbed when the sample was calcined at 500 °C compared to those of 350 °C. For samples prepared in a more alkaline environment, a higher calcination temperature was required to burn the methyl groups than samples prepared at acidic pH.

Final decomposition occurred in higher temperatures in the region of 500 °C-600 °C. The result indicates that the thermal stability of the silica xerogel produced under neutral conditions was higher. This means that the $Si\text{-}CH_3$ group may only decompose at higher temperatures. That is why at higher pH, the surface of silica is more hydrophobic. It is possible that, at a higher pH, more siloxane structures were formed, which protect the methyl group from thermal attack.

3.5. Scanning electron microscopy

Two-dimensional morphological studies of hydrophobic silica thin films were carried out using Scanning Electron Microscopy. The surface morphologies of the DMDM-TEOS silica film at various pH coated on alumina substrates are presented in Fig. 6 at 10,000x magnification. The SEM image shows that the silica film is not homogeneous. As the pH increased, the changes in the fracture morphology of the silica thin films became more clearly visible. With increasing pH, a different texture appears on the surface of the coating. At acidic pH, silica tends to be finer with less cracks on the surface. However, as the pH increases, the silica grains tend to become more numerous and smaller resulting in a rougher surface.

According to the wetting theory proposed by Cassie and Baxter [41], surface roughness is one of the main factors for achieving hydrophobicity. Therefore, low surface energy is mainly caused by hydrocarbon derivatives combined with hydrophobic surface roughness [31]. According to Wenzel, surface roughness increases solid surface area, which geometrically results in increased hydrophobicity. In the Cassie approach, it is stated that air can be trapped under droplets, which leads to hydrophobic behavior because water droplets are partially above the air. Fig. 6 shows the silica coating made at alkaline pH, presenting higher surface roughness, reducing the optical loss produced at acidic pH.

A cross-sectional view is presented in Fig. 6f. SEM images with 500x or 2500x magnification (not presented in Figure) do not clearly show the thickness of the silica layer. The SEM image only shows a cross-sectional image of the alumina substrate. This indicates that the silica layer formed is very thin and, on a nano-meter scale. Previous studies [42–44] report that the thickness of the silica layer is in the range of 200 nm. In this study, the dip-coating and calcination processes were also carried out four times, so it is assumed that the thickness of the silica thin layer is also around 150 nm. Another thing that may happen is that the silica layer enters the pores of the alumina.

3.6. Gas sorption analysis

Fig. 7 shows the nitrogen adsorption isotherms of silica xerogels calcined at 350 °C and 500 °C. The isotherms for each sample cannot be of one specific type due to the heterogeneity of samples. At the calcination temperature of 300 °C, the isotherm showed type IV, indicating that the silica xerogel was in the mesopore range [45]. This isotherm is characterized by a turning point, which indicates the end of the single layer and the beginning of multiple layers' formation. This isotherm type displays the hysteresis loop caused by capillary condensation. At a calcination temperature of 350 °C, all samples except the one prepared at pH 6.44 showed an H4 hysteresis loop with a meager amount of adsorption, implying the low pore volume of the silica xerogel produced, associated with narrow slit pores [46]. These results suggest that the presence of unburnt methyl groups was likely to have clogged pores. A trend was observed with increasing pH starting from 3.92, 4.98, and 6.44, where the amount of nitrogen absorbed increased, though this did not apply to pH 7.21.

In silica xerogels calcined at 500 °C, as shown in Fig. 7b, samples prepared in an acidic atmosphere were dense. High heating caused the silica structure to enclose onto one another. This is in line with the TGA data, which showed that samples prepared under acidic pH had low thermal stability. In contrast, samples prepared at pH 6.44 and 7.21 showed an increase in the volume of N_2 absorbed. In the sample prepared at pH 6.44, the silica pore structure changed from macropore to micropore, and the isotherm showed type 1, which characterizes the microporous material. This result indicates a convergence between the pore width and the pore width of the cell. The amount of nitrogen adsorbed had doubled. Likewise, with silica xerogel prepared at pH

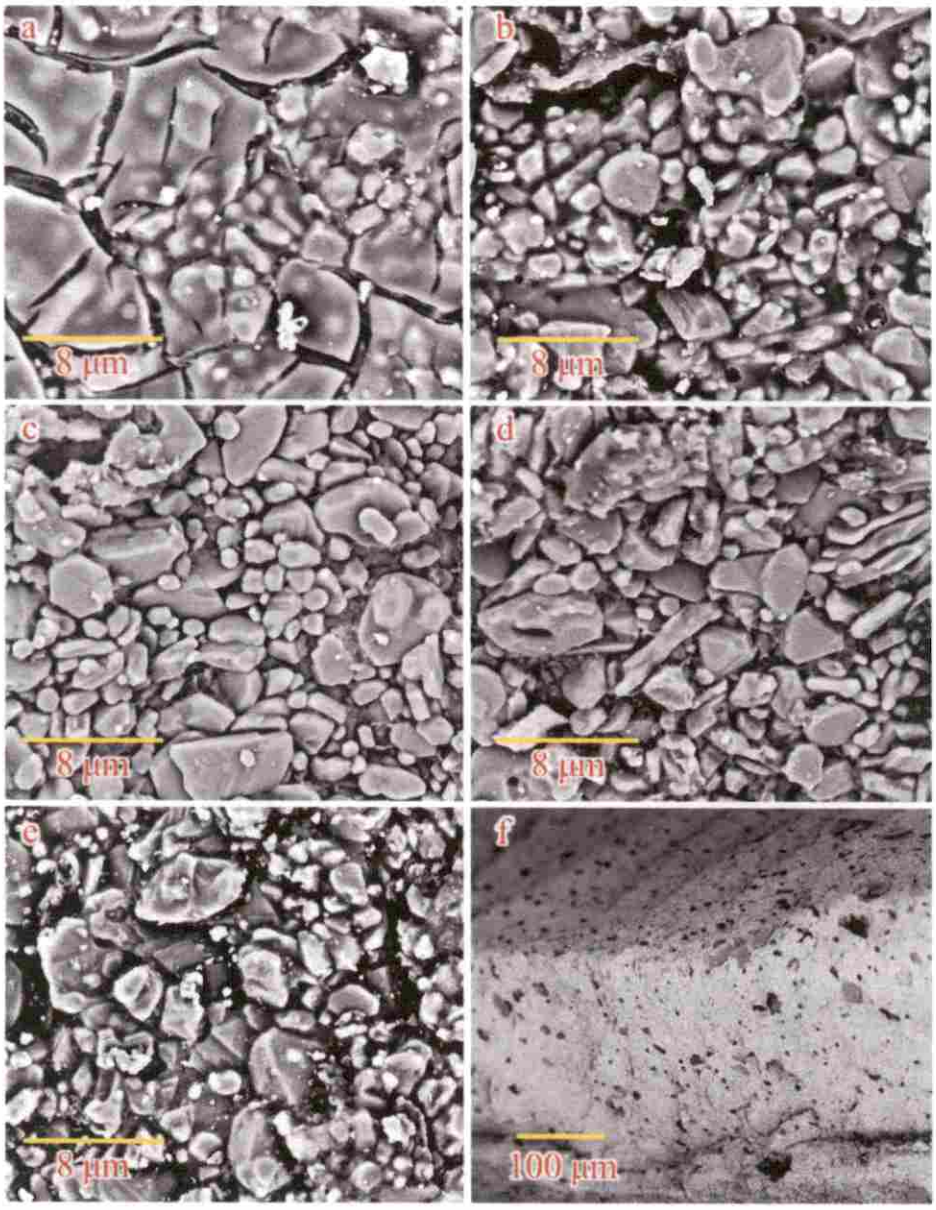

Fig. 6. Scanning electron microscopy images of DMDMS-TEOS silica thin films coated on ceramic plates calcined at 350 °C (a) pH 2.21; (b) pH 3.92 (c) 4.98 (d) 6.44 and (e) 7.21 at 10,000x magnification. Fig. 6f shows the cross-section of the silica film at 500 x magnification.

7.21, there was a multiplied increase in the amount of nitrogen absorbed, from what was previously very low (less than 5 cm^3/g STP) to 180 cm^3/g STP. This result suggests that the calcination process up to 500 °C caused the methyl groups present on the silica surface to be burnt and exposed, thereby opening the clogged pores. Also, higher heating caused further condensation reactions of the remaining Si-OH groups.

At pH 6.44, the pore structure tended to be uniform, signifying that the combustion process produced a uniform pore structure in the micropore region. At pH 7.21, according to the isotherm curve shape, the silica sample can be classified as type H3, in which the hysteresis loop is usually observed due to the aggregation of particles giving rise to slit-shaped pores. This is in line with the presence of silica aggregates, as shown in the SEM image. The combustion process removed the aggregates and pore blockage and then produced meso-sized pores; hence the porosity was formed by gaps between irregular aggregates. The formation of a multilayer film in the pore wall was observed for the curve's initial part. At a relative pressure of more than 0.5, the capillary condensation occurred in the pore structure.

Fig. 8 shows the average pore radius, BET surface area, and pore volume. The average pore radius was about 26 Å (± 5.9 Å), where the mean deviation is not very large. This indicates that the width of the pore size tends to be uniform, especially for samples prepared at acidic pH. As for the 500 °C calcination, the pore radius increased to 46 Å (± 22 Å) with a higher mean deviation. Although the average pore size does not fluctuate much, the pore size distribution is not close. The adsorption isotherm in Fig. 7b shows a different pattern. The silica xerogel isotherm prepared at pH 6.44 shows a combined pattern between Type 1 and Type IV. The surface area was measured up to a pore volume of ~140 (cm^3/g STP) for a total pore volume of 160 (cm^3/g STP), indicating that this material has a relatively large surface area. On the other hand, the prepared silica xerogel isotherm pH 7.21 indicates that the surface area was measured at a pore volume of ~40 (cm^3/g STP) for a total pore volume of ~190 (cm^3/g STP), which means this material has a smaller surface area for a larger pore volume. These results indicate that

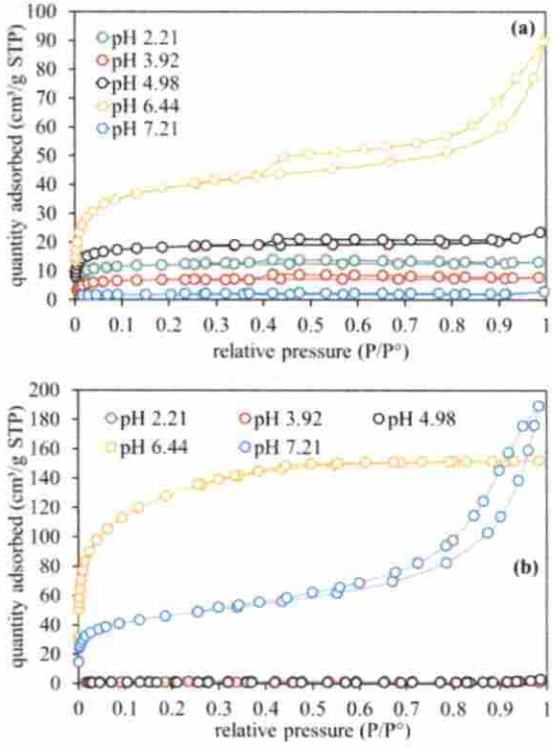

Fig. 7. Nitrogen adsorption isotherms of DMDMS-TEOS silica xerogels at various pH conditions calcined at (a) 350 °C and (b) 500 °C.

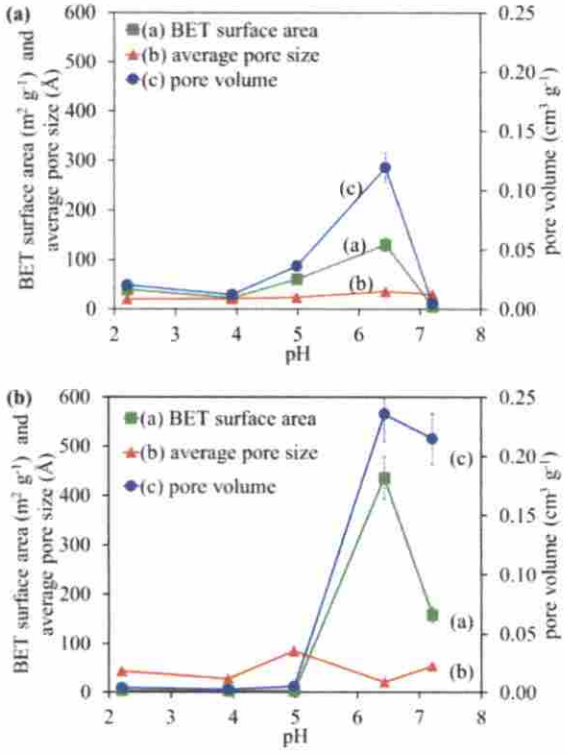

Fig. 8. BET surface area, average pore size, and pore volume of DMDMS-TEOS silica xerogels as a function of pH, calcined at (a) 350 °C and (b) 500 °C.

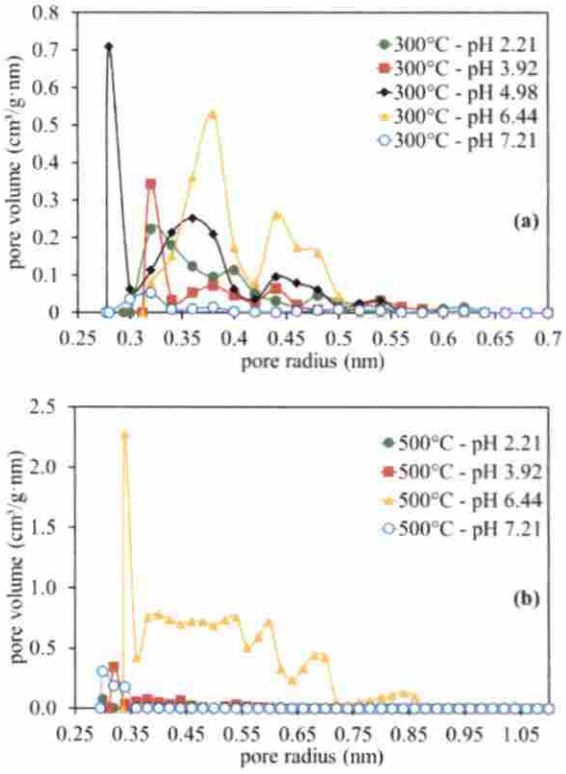

Fig. 9. Pore size distributions of DMDMS-TEOS silica xerogels calcined at (a) 350 °C and (b) 500 °C.

materials prepared at higher pH tend to produce materials with different and broader pore distributions. This result is reinforced by Fig. 9, which shows that at pH 6.44, the pore distribution is wider.

Conversely, at pH 6.44 and 7.21, an increase in calcination temperature upsurge the surface area and pore volume. Synthesis of silica xerogel in neutral pH environments provided good structural stability. In general, lower pH leads to denser materials with smaller average pore sizes, whereas higher pH leads to more porous materials [47, 48]. Low pore volume and high-density gels are formed in a weak cross-linking system in gels prepared under acidic conditions. Meanwhile, gel prepared under alkaline conditions produce silica polymer that is larger and more cross-linked [48]. The pore volume and surface area of silica xerogels calcined at 500 °C were about two times higher than those calcined at 350 °C. These results imply that removing pore blockage was more than the process of material shrinkage caused by an increase in calcination temperature.

The size distributions of the silica xerogels are shown in Fig. 9. The pore size was calculated based on the MP method. The narrow pore size distribution at 0.25 to 0.6 nm confirmed that the silica xerogel was in the micropore region. This result was smaller than the average pore size (diameter 26 Å (2.6 nm) or radius 13 Å (1.3 nm) data. Larger mesoporous pores were not detected in the nitrogen adsorption. These results specify the silica produced as a viable molecular sieve for the desalination process. However, this result makes sense because the average pore diameter also calculates large pores in this material. In silica calcined at 500 °C, a significant change of slightly widening to 0.85 nm in the pore size distribution was observed, especially in the sample prepared at pH 6.44. This shows that the combustion process produced larger pores.

3.7. Desalination performance

Fig. 10 shows the DMDMS-TEOS silica membrane desalination

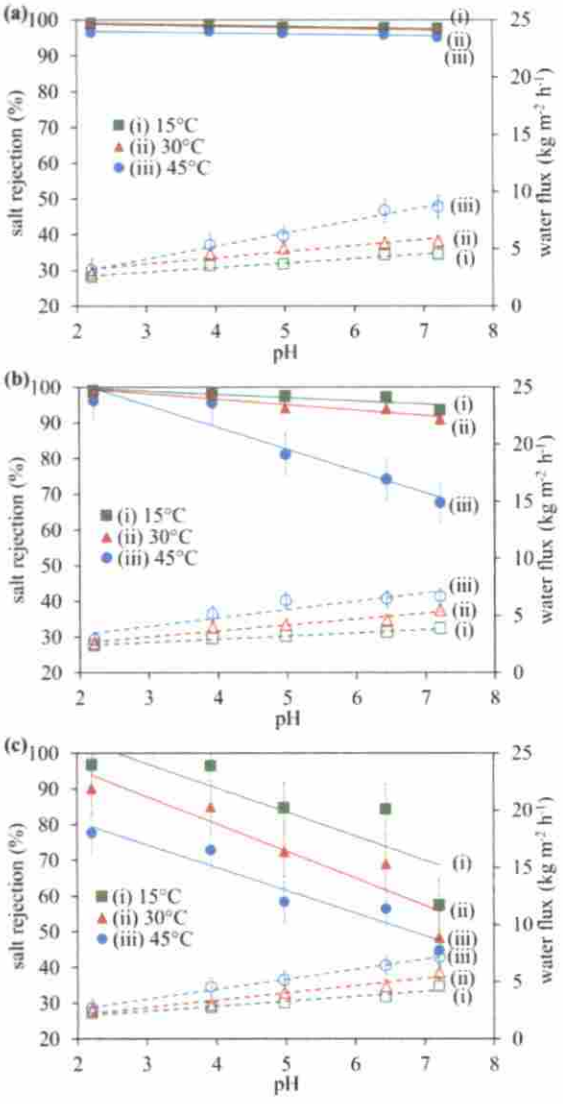

Fig. 10. Salt rejection (filled bullet) and water flux (empty bullet) of DMDMS-TEOS silica membranes at NaCl concentrations of (a) 0.3 wt.% (b) 1 wt.% (c) 3.5 wt.%.

Table 2
Desalination performance of several types of silica membranes.

Membrane type	Feed temp. (°C)	Feed concentration (%)	Water flux (kg.m^{-2}.h^{-1})	Salt rejection (%)	Ref.
DMDMS-TEOS silica membrane	15–45	0.3–3.5	2–9	99	This work
Si-P123 calcined at 350 °C	25–60	0.3–5	1.1–5.6	99.2	[49]
Hybrid membrane	25–60	1–15	2.3–5.7	>99.7	[50]
Carbonized C16 silica template	60	0.3–3.5	2.1–3.1	91–97%	[17]
Hybrid TEVS-P123	60	0.3	3.7	>95	[14]
Silica-cobalt	22–60	0.3–7.5	0.6–25.8	>90	[20]

performance as a function of pH, salt concentration, and salt solution temperature. In general, all DMDMS-TEOS silica membranes produced high water fluxes of up to 9 kg m^{-2} h^{-1} with good salt rejection reaching values above 99%, particularly at a salt concentration of 0.3 wt.%. However, salt rejection declined with increasing salt concentration. Table 2 shows a summary of membranes' performance in this study along with other silica membranes synthesized in other studies for desalination. The membrane performances in this work were relatively high, indicated by the water fluxes produced, which reached 9 kg m^{-2} h^{-1}. These results are comparatively better than other membranes. The water fluxes produced were only lower than the cobalt silica membrane prepared by Elma, Wang, Yacou, Motuzas and Diniz da Costa [20]. The DMDMS-TEOS membranes in this work showed good flux performance. This may be due to the methyl group that produced a larger pore compared to other membranes.

With increasing pH, the water flux rose for all salt concentrations and treatment temperatures. However, the performance of salt rejection was inversely proportional. This is understandable as there is always a seesaw between quality and productivity. When production increases, the quality cuts, and vice versa. The increase in water flux with increasing pH, which is applied to all salt concentration variations, is in line with the results of nitrogen adsorption measurements, showing that pore volume and surface area increased with increasing pH. Membranes prepared at a lower pH gave better salt rejection than those prepared at a more alkaline pH because, at a lower pH, the resulting structure was denser, with narrower pore size. These results are consistent with what was described in the previous nitrogen absorption discussion. Also, SEM images clearly showed that a lower pH resulted in a smoother and denser structure, while a higher pH tended to result in a cracked silica layer. Fig. 10 also proves that the silica membrane functioned well in carrying out the process of pervaporation. This is characterized by better water flux performance at higher desalination temperatures where 45 °C>30 °C>15 °C, confirming that the desalination occurred through a pervaporation mechanism. The increasing temperature of the saline solution increased the vapor pressure, and thus the water molecules obtained more thermal energy to overcome the energy barrier at the pore entrance.

Based on the SEM images, membrane performance, and material characterizations, we propose a theory that lower pH results in silica membranes with smaller gaps or pores than membranes prepared under more alkaline conditions, as illustrated schematically in Fig. 11. It should be noted that the pores overlap, forming narrower pore blocks that are selective to Na^+ and Cl^- ions. In this study, testing for higher salt concentrations was carried out after lower salt concentrations. Repeated use caused water flow in the pore walls to significantly erode the silica

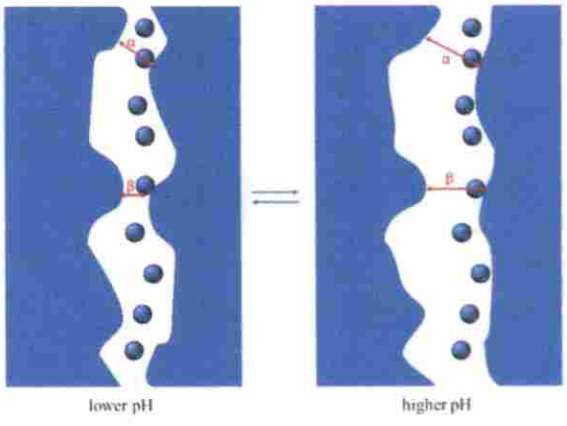

Fig. 11. Schematic of changes in porosity in membranes prepared under acidic and alkaline conditions. (For interpretation of the references to colour in this figure legend, the reader is referred to the web version of this article.)

layer, which resulted in lower membrane performance.

Although the pore size of silica given by nitrogen adsorption was greater than the size of water molecules (d_k = 2.6 Å) and hydrated salt ions Na^+: d_k = 7.2 Å and Cl^-: d_k = 6.6 Å) [9], the silica membranes could still carry out the pervaporation processes. A possible reason to explain this is that even though the silica was thin (thickness of about 100–200 nm), the silica pores were arranged such that they imposed one another so that there was a sieve above the sieve. This resulted in an effective pore diameter in the thin layer rather than a pore diameter in the xerogel.

4. Conclusions

Xerogel and silica thin films have been made from dimethyldimethoxysilane (DMDMS) - tetraethylorthosilicate (TEOS) using a sol-gel method with pH variations. The effect of pH from acid to neutral was investigated on the physical and chemical properties of xerogel, thin layer hydrophobicity, and desalination performance with variations in temperature and brine concentration. The characterization results show that membranes prepared under neutral conditions produced desirable properties such as higher thermal stability, greater pore volume, thermal stability, and higher hydrophobicity. For the desalination process, the silica membrane achieved excellent separation performance (>99%), especially for low salt concentrations. As the pH increased, the water flux increased, but the salt rejection decreased. The membrane works for desalination through the mechanism of pervaporation.

CRediT authorship contribution statement

Adi Darmawan: Conceptualization, Resources, Investigation, Data curation, Formal analysis. **Linda Karlina:** Investigation, Data curation. **Ika Khairunnisak:** Investigation, Data curation, Writing – original draft. **Riza Eka Saputra:** Formal analysis, Visualization, Writing – review & editing. **Choiril Azmiyawati:** Supervision, Writing – review & editing. **Yayuk Astuti:** Resources, Writing – review & editing. **S. Sriatun:** Supervision, Writing – review & editing. **Avior Puspa Noorita:** Conceptualization.

Declaration of Competing Interest

The authors declare that they have no known competing financial interests or personal relationships that could have appeared to influence the work reported in this paper.

Acknowledgment

The authors gratefully acknowledge Diponegoro University's financial support via the Research for International Scientific Publications Award (Number: 572-04/UN7.5.1/PG/2016). Special thanks are also due to the FIMlab at the University of Queensland for the support in sample analysis. Thanks to Wiji Rahayu from DKSH Indonesia for her assistance on the zeta potential analysis.

References

[1] E. Drioli, A.I. Stankiewicz, F. Macedonio, Membrane engineering in process intensification—An overview, J Memb Sci 380 (2011) 1–8.
[2] M.C. Duke, J. O'Brien-Abraham, N. Milne, B. Zhu, J.Y.S. Lin, J.C. Diniz da Costa, Seawater desalination performance of MFI type membranes made by secondary growth, Sep. Purif. Technol. 68 (2009) 343–350.
[3] C. Charcosset, A review of membrane processes and renewable energies for desalination, Desalination 245 (2009) 214–231.
[4] S. Lee, C. Boo, M. Elimelech, S. Hong, Comparison of fouling behavior in forward osmosis (FO) and reverse osmosis (RO), J Memb Sci 365 (2010) 34–39.
[5] M. Elma, C. Yacou, D.K. Wang, S. Smart, J.C. Diniz da Costa, Microporous Silica Based Membranes for Desalination, Water (Basel) 4 (2012) 629–649.
[6] C.H. Cho, K.Y. Oh, S.K. Kim, J.G. Yeo, P. Sharma, Pervaporative seawater desalination using NaA zeolite membrane: mechanisms of high water flux and high salt rejection, J Memb Sci 371 (2011) 226–238.
[7] D. Uhlmann, S. Smart, J.C. Diniz da Costa, H_2S stability and separation performance of cobalt oxide silica membranes, J Memb Sci 380 (2011) 48–54.
[8] C. Yacou, S. Smart, J.C. Diniz da Costa, Long term performance cobalt oxide silica membrane module for high temperature H_2 separation, Energy Environ. Sci. 5 (2012) 5820–5832.
[9] L. Li, J. Dong, T.M. Nenoff, R. Lee, Reverse osmosis of ionic aqueous solutions on a MFI zeolite membrane, Desalination 170 (2004) 309–316.
[10] C.J. Brinker, G.W. Scherer, Sol-Gel Science: The Physics and Chemistry of Sol-Gel Processing, Academic press, 1990.
[11] R. Leboda, E. Mendyk, Hydrothermal modification of porous structure of silica adsorbents, Mater. Chem. Phys. 27 (1991) 189–212.
[12] R.K. Iler, The Chemistry of Silica: Solubility, Polymerization, Colloid and Surface Properties and Biochemistry of Silica, Wiley, 1979.
[13] G. Li, M. Kanezashi, T. Tsuru, Preparation of organic–inorganic hybrid silica membranes using organoalkoxysilanes: the effect of pendant groups, J Memb Sci 379 (2011) 287–295.
[14] B.P. Ladewig, Y.H. Tan, C.X.C. Lin, K. Ladewig, J.C. Diniz da Costa, S. Smart, Preparation, Characterization and Performance of Templated Silica Membranes in Non-Osmotic Desalination, Materials (Basel) 4 (2011) 845.
[15] M. Elma, D.K. Wang, C. Yacou, J.C. Diniz da Costa, Interlayer-free P123 carbonised template silica membranes for desalination with reduced salt concentration polarisation, J Memb Sci 475 (2015) 376–383.
[16] M.C. Duke, S. Mee, J.C.D. da Costa, Performance of porous inorganic membranes in non-osmotic desalination, Water Res. 41 (2007) 3998–4004.
[17] S. Wijaya, M.C. Duke, J.C. Diniz da Costa, Carbonised template silica membranes for desalination, Desalination 236 (2009) 291–298.
[18] Y.T. Chua, C.X.C. Lin, F. Kleitz, X.S. Zhao, S. Smart, Nanoporous organosilica membrane for water desalination, Chem. Commun. 49 (2013) 4534–4536.
[19] C.X.C. Lin, L.P. Ding, S. Smart, J.C. Diniz da Costa, Cobalt oxide silica membranes for desalination, J. Colloid Interface Sci. 368 (2012) 70–76.
[20] M. Elma, D.K. Wang, C. Yacou, J. Motuzas, J.C. Diniz da Costa, High performance interlayer-free mesoporous cobalt oxide silica membranes for desalination applications, Desalination 365 (2015) 308–315.
[21] A. Darmawan, L. Karlina, Y. Astuti, J. Sriatun, D.K. Motuzas, J.C. Wang, Costa Diniz da, Structural evolution of nickel oxide silica sol-gel for the preparation of interlayer-free membranes, J. Non Cryst. Solids 447 (2016) 9–15.
[22] J.-H. Moon, J.-H. Bae, Y.-S. Bae, J.-T. Chung, C.-H. Lee, Hydrogen separation from reforming gas using organic templating silica/alumina composite membrane, J Memb Sci 318 (2008) 45–55.
[23] J. Campaniello, C.W.R. Engelen, W.G. Haije, P.P.A.C. Pex, J.F. Vente, Long-term pervaporation performance of microporous methylated silica membranes, Chem. Commun. (2004) 834–835.
[24] Q. Wei, F. Wang, Z.-R. Nie, C.-L. Song, Y.-L. Wang, Q.-Y. Li, Highly Hydrothermally Stable Microporous Silica Membranes for Hydrogen Separation, J. Phys. Chem. B 112 (2008) 9354–9359.
[25] A.P. Rao, A.V. Rao, G.M. Pajonk, Hydrophobic and physical properties of the ambient pressure dried silica aerogels with sodium silicate precursor using various surface modification agents, Appl. Surf. Sci. 253 (2007) 6032–6040.
[26] R.E. Saputra, Y. Astuti, A. Darmawan, Hydrophobicity of silica thin films: the deconvolution and interpretation by Fourier-transform infrared spectroscopy, Spectrochim. Acta Part A 199 (2018) 12–20.
[27] H. Jiang, Z. Zheng, J. Xiong, X. Wang, Studies on dialkoxysilane hydrolysis kinetics under alkaline conditions, J. Non Cryst. Solids 353 (2007) 4178–4185.
[28] K. Kusakabe, F. Shibao, G. Zhao, K.-I. Sotowa, K. Watanabe, T. Saito, Surface modification of silica membranes in a tubular-type module, J Memb Sci 215 (2003) 321–326.
[29] M.A. Karakassides, D. Gournis, D. Petridis, An infrared reflectance study of Si–O vibrations in thermally treated alkali-saturated montmorillonites, Clay Miner. 34 (1999) 429–429.
[30] P.G. Pawar, R. Xing, R.C. Kambale, A.M. Kumar, S. Liu, S.S. Latthe, Polystyrene assisted superhydrophobic silica coatings with surface protection and self-cleaning approach, Prog. Org. Coat. 105 (2017) 235–244.
[31] D. Le, S. Kongparakul, C. Samart, P. Phanthong, S. Karnjanakom, A. Abudula, G. Guan, Preparing hydrophobic nanocellulose-silica film by a facile one-pot method, Carbohydr. Polym. 153 (2016) 266–274.
[32] S.A. Kulkarni, S.B. Ogale, K.P. Vijayamohanan, Tuning the hydrophobic properties of silica particles by surface silanization using mixed self-assembled monolayers, J. Colloid Interface Sci. 318 (2008) 372–379.
[33] A. Nakajima, K. Hashimoto, T. Watanabe, Recent studies on super-hydrophobic films, Monatshefte für Chemie/Chemical Monthly 132 (2001) 31–41.
[34] H. Homma, T. Kuroyagi, K. Izumi, C.L. Mirley, J. Rouzello, S.A. Boggs, Diffusion of low molecular weight siloxane from bulk to surface, IEEE Trans. Dielectr. Electr. Insul. 6 (1999) 370–375.
[35] A. Darmawan, S.A. Rasyid, Y. Astuti, Modification of the glass surface with hydrophobic silica thin layers using tetraethylorthosilicate (TEOS) and trimethylchlorosilane (TMCS) precursors, Surf. Interface Anal. 53 (2021) 305–313.
[36] V.C. Farmer, J.D. Russell, The infra-red spectra of layer silicates, Spectrochim. Acta 20 (1964) 1149–1173.
[37] A. Darmawan, R.Eka Saputra, Y. Astuti, Structural, thermal and surface properties of sticky hydrophobic silica films: effect of hydrophilic and hydrophobic precursor compositions, Chem. Phys. Lett. 761 (2020), 138076.
[38] L. Karlina, C. Azmiyawati, A. Darmawan, Synthesis and characterization of hydrophobic silica prepared by different acid catalysts, IOP Conference Series: Materials Science and Engineering 509 (2019), 012065.

[39] A. Darmawan, L. Karlina, Y. Astuti, Sriatun, D.K. Wang, J. Motuzas, J.C.D. da Costa, Interlayer free – nickel doped silica membranes for desalination, in: IOP Conference Series: Materials Science and Engineering 172, 2017, 012001.
[40] C.J. Brinker, Hydrolysis and condensation of silicates: effects on structure, J. Non Cryst. Solids 100 (1988) 31–50.
[41] A.B.D. Cassie, S. Baxter, Wettability of porous surfaces, Trans. Faraday Soc. 40 (1944) 546–551.
[42] A. Darmawan, J. Motuzas, S. Smart, A. Julbe, J.C. Diniz da Costa, Binary iron cobalt oxide silica membrane for gas separation, J Memb Sci 474 (2015) 32–38.
[43] B.A. McCool, N. Hill, J. DiCarlo, W.J. DeSisto, Synthesis and characterization of mesoporous silica membranes via dip-coating and hydrothermal deposition techniques, J Memb Sci 218 (2003) 55–67.
[44] E. Volentiru, M. Nyári, G. Szabó, Z. Hórvölgyi, L.M. Muresan, Silica sol–gel protective coatings against corrosion of zinc substrates, Periodica Polytechnica Chemical Engineering 58 (2014) 61–66.
[45] K.S.W. Sing, D.H. Everett, R.A.W. Haul, L. Moscou, R.A. Pierotti, J. Rouquerol, T. Siemieniewska, Reporting physisorption data for gas/solid systems with special reference to the determination of surface area and porosity (Recommendations 1984), Pure Appl. Chem. (1985) 603–619.
[46] S. Lowell, J.E. Shields, M.A. Thomas, M. Thommes, Characterization of Porous Solids and Powders: Surface Area, Pore Size and Density, Springer, Netherlands, 2012.
[47] L.L. Hench, W. Vasconcelos, Gel-Silica Science, Annu. Rev. Mater. Sci. 20 (1990) 269–298.
[48] A.M. Buckley, M. Greenblatt, The Sol-Gel Preparation of Silica Gels, J. Chem. Educ 71 (1994) 599.
[49] A. Rahma, M. Elma, E.L.A. Rampun, A.E. Pratiwi, A. Rakhman, Fitriani, Rapid Thermal Processing and Long Term Stability of Interlayer-free Silica-P123 Membranes for Wetland Saline Water Desalination, Journal of Advanced Research in Fluid Mechanics and Thermal Sciences 71 (2020) 1–9.
[50] H. Yang, D.K. Wang, J. Motuzas, J.C. Diniz da Costa, Hybrid vinyl silane and P123 template sol–gel derived carbon silica membrane for desalination, J Solgel Sci Technol 85 (2018) 280–289.